Acta Oceanol. Sin., 2013, Vol. 32, No. 1, P. 79-88
DOI: 10.1007/s13131-013-0269-5
http://www.hyxb.org.cn
E-mail: hyxbe@263.net

Areas of the global major river plumes

KANG Yan[1,2], PAN Delu[1,2*], BAI Yan[2], HE Xianqiang[2], CHEN Xiaoyan[1,2],

CHEN Chen-Tung Arthur[3], WANG Difeng[2]

[1] Department of Earth Sciences, Zhejiang University, Hangzhou 310027, China
[2] State Key Laboratory of Satellite Ocean Environment Dynamics, Second Institute of Oceanography, State Oceanic Administration, Hangzhou 310012, China
[3] Institute of Marine Geology and Chemistry, National Sun Yat-sen University, Kaohsiung, Taiwan 804, China

Received 1 April 2012; accepted 18 September 2012

Abstract
River plumes are the regions where the most intense river-sea-land interaction occurs, and they are characterized by complex material transport and biogeochemical processes. However, due to their highly dynamic nature, global river plume areas have not yet been determined for use in synthetic studies of global oceanography. Based on global climatological monthly averaged salinity data from the NOAA World Ocean Atlas 2009 (WOA09), and monthly averaged salinity contour maps of the East and South China Seas from the Chinese Marine Atlas, we extract the monthly plume areas of major global rivers using a geographic information system (GIS) technique. Only areas with salinities that are three salinity units lower than the average salinity in each ocean are counted. This conservative estimate shows that the minimum and maximum monthly values of the total plume area of the world's 19 largest rivers are 1.72×10^6 km^2 in May and 5.38×10^6 km^2 in August. The annual mean area of these river plumes (3.72×10^6 km^2) takes up approximately 14.2% of the total continental shelves area worldwide (26.15×10^6 km^2). This paper also presents river plume areas for different oceans and latitude zones, and analyzes seasonal variations of the plume areas and their relationships with river discharge. These statistics describing the major global river plume areas can now provide the basic data for the various flux calculations in the marginal seas, and therefore will be of useful for many oceanographic studies.
Key words: river plume, World Ocean Atlas, geography information system, Changjiang River, marginal sea

Citation: Kang Yan, Pan Delu, Bai Yan, He Xianqiang, Chen Xiaoyan, Chen Chen-Tung Arthur, Wang Difeng. 2013. Areas of the global major river plumes. Acta Oceanologica Sinica, 32(1): 79–88, doi: 10.1007/s13131-013-0269-5

1 Introduction

The global freshwater discharge from rivers into the oceans is about 36 109 km^3/a (GRDC, 2009), and approximately 40% of the freshwater and particulate material transported into the oceans is from the top ten largest rivers (Dagg et al., 2004; Chen et al., 2008). Large rivers generate offshore plumes characterized by high buoyancy and biological productivity because of their low salinities, high levels of nutrients, suspended and dissolved terrestrial materials (Higgins et al., 2006; Kouame et al., 2009), As a result, the chemical, geological, biological and physical environments of adjacent marginal seas are affected (Smith and Demaster, 1996; Shipe et al., 2006).

River plumes are important locations where land and ocean processes meet, but they are not as well understood as other areas of the world's ocean. River plumes can travel long distances and are known to be high in biological productivity, because of their nutrient input, making the adjacent shelves important fishing grounds. River plumes also transport terrestrial material to the shelves and beyond, and are important in sediment distribution, as well as in affecting the distribution of pollutants and the biogeochemistry of carbon and associated elements. High phytoplankton productions cause eutrophication and may even generate hypoxia, which may lead to the establishment of dead zones in the coastal area (Diaz and Rosenberg, 2008). Many studies show that large river plumes are atmospheric CO_2 sinks due to the combination of biological and physical processes occurring in them, but the air-sea CO_2 fluxes vary significantly with seasons (Cai, 2003; Tan et al., 2004; Green et al., 2006; Cooley et al., 2007; Zhai and Dai, 2009; Zhai et al., 2009). Based on extensive research on air-sea CO_2 exchange in 106 estuaries, Chen et al. (2012) pointed out that estuaries are CO_2 sources, while the large river plumes become a CO_2 sink even many hundred kilometers beyond the river mouth. However, a study of how important these plumes are in terms of the carbon cycle, for instance, has not been possible because of the lack of detailed information on the exact plume areas. Therefore, the determination of major river plume areas is urgently needed for the assessments of the global oceanic carbon budget and other flux estimations. Yet, owing to the highly dynamic nature of plume systems but the limited extent of field investigations in them, even the plume areas of the world's major rivers are not available, not to mention their spatial and temporal

Foundation item: The National Basic Research Program of China (973 Program) under contract No. 2009CB421202; the Public Science and Technology Research Funds Projects of Ocean under contract No. 200905012; the National Natural Science Foundation of China under contract Nos 41271378, 40976110 and 40706061; the National High Technology Research and Development Program of China (863 Program) under contract No. 2007AA092201.
*Corresponding author, E-mail: pandelu@sio.org.cn

characteristics.

Recently, two specific microwave satellite sensors (L-band radiometers) were launched to monitor surface water salinity for the global ocean: the SMOS (the Soil Moisture and Ocean Salinity) and Aquarius/SAC-D satellite. These two microwave satellite sensors are good for open ocean observations over a very large scale. Nevertheless, because of their coarse spatial resolution (typically 30–300 km) and long revisiting time (3 d or more) (Koblinsky et al., 2003; Font and Camps, 2010; Kerr et al., 2010), they are still of limited capacity for the observation of salinity in coastal areas. Satellite ocean color data with relatively higher spatial resolution (e.g., ~1–9 km) and revisiting frequency (e.g., less than 1 d) has also been used to detect some larger river plumes based on the difference of water color between plume and ambient waters (Klemas, 2012). Several methods have been used to study the spatial and temporal variations of some large river plumes because there are good relationships between salinity and the absorption coefficients of dissolved organic matter and detritus, which can be retrieved by satellite ocean color data (Binding and Bowers, 2003; D'Sa and Miller, 2003; Hu et al., 2004; Vecchio and Subramaniam, 2004; Chen et al., 2007). Satellite-derived chlorophyll concentration and diffuse attenuation coefficient from MODIS (Moderate Resolution Imaging Spectroradiometer) and SeaWiFS (Sea-viewing Wide Field-of-view Sensor) were also used to characterize the variability of river plumes, such as the La Plata River plume (Piola et al., 2008), the Chesapeake Bay estuarine outflow (Dzwonkowski and Yan, 2005), the Amazon River plumes (Jo et al., 2005; Cooley et al., 2007; Molleri et al., 2010), and the Changjiang River (Kim et al., 2009). Meanwhile, the satellite-retrieved normalized water-leaving radiances (Thomas and Weatherbee, 2006; Lihan et al., 2008) and sea surface temperature from NOAA Advanced Very High Resolution Radiometer (AVHRR) data (Walker, 1996) were also used to detect the river plumes. However, all these methods were established based on regional data and specified for local systems, which cannot be extended easily to estimate the global river plume areas because different rivers may have different optical characteristics, and it is difficult to use the same satellite algorithm and criteria to define all river plumes.

In contrast, the available synthesized data sets of global oceanic salinity enable us to obtain the climatological distributions of the global major river plumes. Therefore, the goal of this paper is to use the global in situ salinity data set from the World Ocean Atlas 2009 (WOA09) provided by NOAA (National Oceanic and Atmospheric Administration) (Antonov et al., 2010) and the salinity contour maps of the East and South China Seas from the Chinese Marine Atlas (Chen, 1992; Hon, 2006) to extract the climatological monthly averaged plume areas of major rivers based on the Geographic Information System (GIS) technology. GIS spatial analysis technology has a higher accuracy and credibility for calculating the area of river plumes compared with other methods. It should be pointed out that, although the two ocean atlas data sets we used are climatologies, they are still sufficient to create global statistics, which did not exist for the various plume-related flux calculations and other multipledisciplinary oceanographic studies.

In this paper, we present the data acquisition and extraction method for plume areas in Section 2. In Section 3, we provide the plume areas of major rivers and statistical data for different oceans and latitude zones. We also analyze the seasonal variations of plume areas and their relationships with the river discharge. Finally, we discuss the implications of the extracted plume areas for future work in Section 4.

2 Data and methods

2.1 *Data acquisition*

(1) Basic geographic information data

We obtained basic geographic information data from the Natural Earth data set (http://www.naturalearthdata.com/), including the ocean, land and rivers maps. The Natural Earth dataset is a free, public domain map available in vector and raster formats with 1:10 000 000, 1:50 000 000, and 1: 110 000 000 scales. Here, we use the 10 m_land, 10 m_ocean, 10 m_river_lake_centerlines, and 10 m_bathymetry datasets, where 10 m equates to a 1:10 000 000 scale of the relative data set.

The total area of the global continental shelves calculated in this paper is 26.15×10^6 km^2 (with water depth < 200 m), which is between the minimum value used by Cai et al. (2006) (25.83×10^6 km^2) and the maximum value used by Chen and Borges (2009) (30.0×10^6 km^2).

(2) Global salinity data

We obtained the NOAA World Ocean Atlas 2009 (WOA09) salinity data from its website (http://www.nodc.noaa.gov/OC5/SELECT/woaselect/woaselect.html) using the WOAselect tool (Antonov et al., 2010). WOAselect is an interactive tool which enables the user to view the climatological monthly averaged data by designating a specific area, depth, resolution, file format and oceanographic variable. The salinity data have a spatial resolution of 0.25° in the GIS point vector file format. The WOA09 salinity data set has 24 layers, and we only use the surface layer of data.

In addition, we used the monthly averaged salinity contour maps from the China Marine Atlas in the East and South China Seas (Chen, 1992; Hon, 2006) to get more detail for the plume areas of the Changjiang River and Zhujiang River (Pearl River). We digitized the Atlas maps to raster images. Then we established their location in terms of map projections using ArcGIS software. In ArcGIS, we used Geo-referencing and Vectorizing processes to obtain salinity contour data.

(3) Global major river information

The discharges of the world's top 25 largest rivers (ranked in terms of discharge) are taken from McKee et al. (2003), as shown in Table 1. The total discharge of these 25 rivers is about 17 440 km^3/a, and the total accounts for 48.3% of the total freshwater discharge into the oceans from rivers. In this study, we only include the plume areas of 19 rivers since the WOA09 data set lacks the effective salinity data in the other six river estuaries (Mekong, Magdalena, Purari, Indus, Zambezi and Danube). The locations of these 19 rivers are shown in Fig.1. The total discharge of these 19 rivers is approximately 15 910 km^3/a, and accounts for 44.06% of the total freshwater into the oceans.

2.2 *Extraction method of the global major river plume areas*

(1) Threshold salinity for identification of river plume area

The threshold salinity values for the identification of river plume areas are different from ocean to ocean, since different ocean basins have different background salinities. Using the WOA09 salinity data set, we determined the monthly mean surface layer salinities for all five oceans, and the results are given in Table 2. Although there are slight monthly variations, the Atlantic Ocean has the highest salinity, and the Pacific Ocean has the lowest mean surface salinity next to the Arctic Ocean. Surface layer salinity is quite low in the Arctic Ocean because of the large freshwater input from rivers, low evaporation, and seasonal ice melt (Lique et al., 2011). The annual-mean surface layer salinities are 34.51, 34.98, 34.77 and 30.00 for the Pacific Ocean, Atlantic Ocean, Indian Ocean and Arctic Ocean, respectively.

For the purpose of the river plume identification, we took the threshold salinity values for the river plume boundary to be 31, 32, 32 and 27 for the Pacific Ocean, Atlantic Ocean, Indian Ocean and Arctic Ocean, respectively, which are about three salinity units lower than the corresponding annual-mean salinities for each ocean. We use a very conservative threshold considering the areas with significant influence by freshwater. For comparison, we also provide data with the various thresholds for individual river plume. In addition, for some relatively small rivers, the plume areas are too small to be detected by the WOA09 data set during the dry season, and for such cases, the river plume area is neglected.

(2) River plume area extraction by GIS technique

Both the basic geographic information and salinity data

Table 1. The discharges of world's largest 25 rivers (data from McKee et al., 2003)

Oceans	River	Discharge/$10^9 m^3 \cdot a^{-1}$	Rank	Total discharge/$10^9 m^3 \cdot a^{-1}$
Atlantic Ocean	Amazon	6 300	1	10 630
	Congo	1 250	2	
	Orinoco	1 200	3	
	Mississippi	530	7	
	Paraná	470	10	
	Saint Lawrence	450	11	
	Magdalena[1)]	240	20	
	Niger	190	24	
Pacific Ocean	Chang Jiang	900	5	2 590
	Mekong[1)]	470	9	
	Amur	325	14	
	Pearl	300	16	
	Columbia	250	18	
	Yukon	195	23	
	Purari/Fly[1)]	150	25	
Indian Ocean	Ganges and Brahmaputra	970	4	2 160
	Irrawaddy	430	12	
	Salween	300	17	
	Indus[1)]	240	19	
	Zambezi[1)]	220	21	
Arctic Ocean	Yenisei	630	6	1 850
	Lena	510	8	
	Ob	400	13	
	Mackenzie	310	15	
Black Sea	Danube[1)]	210	22	210
Total discharge/$10^9 m^3 \cdot a^{-1}$		15 910[2)]		17 440

Notes: [1)] The six rivers are not calculated because the WOA09 data set lacks the effective salinity data in their estuaries. [2)] Total discharge for the 19 rivers only.

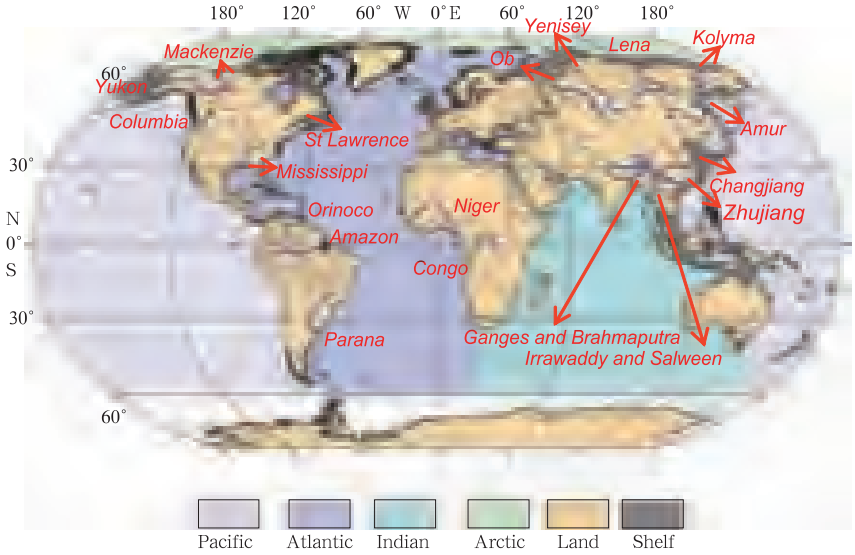

Fig.1. Locations of the world's 19 major rivers.

Table 2. Monthly mean surface water salinities of different oceans from the WOA09 data set

Month	Pacific	Atlantic	Indian	Arctic
January	34.52	35.05	34.76	30.34
February	34.54	35.08	34.74	30.25
March	34.54	35.08	34.74	30.44
April	34.54	35.06	34.72	30.86
May	34.53	35.01	34.74	30.53
June	34.52	34.93	34.79	29.65
July	34.49	34.84	34.82	28.70
August	34.47	34.84	34.78	29.05
September	34.48	34.93	34.77	29.85
October	34.48	34.98	34.79	29.93
November	34.49	34.99	34.81	30.02
December	34.50	35.01	34.79	30.40
Annual mean	34.51	34.98	34.77	30.00

were loaded into the ArcGIS software, and mapped with the same coordinates and projection method (World_Cylindrical_Equal_Area) using the "Projections and Transformations" tool of ArcGIS. Then, the regions with salinity less than the seven threshold salinities ($S \leqslant 26$, $S \leqslant 27$, $S \leqslant 28$, $S \leqslant 29$, $S \leqslant 30$, $S \leqslant 31$ and $S \leqslant 32$) were extracted using the ArcGIS "extraction" spatial analysis tool for each monthly salinity data set, and reclassified with the ArcGIS "reclassify" tool to obtain binary data in which the plume cells were marked as "1" and non-plume cells were marked as "0". Then, the plume grids were converted into polygon features using the ArcGIS "Raster to the Polygon" raster-vector conversion tool and the "area" field was added to the attribute table of the feature class using the ArcGIS "Add Field" tool. The ArcGIS tool "Calculate Geometry" tool was used to automatically calculate the area of each polygon feature in the feature, and the results were stored in the "area" field. Finally, the ArcGIS "Zonal" tool was used to summarize the above area values and to report the results.

3 Results and discussion

3.1 *Statistics of the global major river plume areas*

Table 3 gives the monthly plume areas for all the world's 19 major rivers. It should be noted that the plume areas in the Arctic Ocean are strongly affected by ice melts in addition to river input. Except for the river plumes in the Arctic Ocean, the combined plumes of the Ganges and Brahmaputra, Irrawaddy, and Salween Rivers have the largest annual-mean area because the Bay of Bengal is included. Also, the Saint Lawrence River has the second largest annual-mean plume area because the Gulf of Saint Lawrence, one of the largest estuaries in the world, is included. The Changjiang River and Amazon River have the similar annual-mean plume areas, although the annual discharge of the Amazon River is about seven times larger than that of the Changjiang River (Table 1). This indirectly indicates that the plume area is not only controlled by the river discharge, but it is also modulated by the surrounding topography, among other things. In general, the annual-mean total plume area of the 19 rivers is 3.72×10^6 km^2, and it takes approximately 14.2% of the global continental shelves area (26.15×10^6 km^2).

Table 4 gives the monthly plume areas statistics grouped by the receiving oceans and latitude zones for the 19 rivers. Except for the Arctic Ocean which is affected by ice melt, the Atlantic Ocean (which receives seven rivers) has the largest annual-mean plume area of $1\ 141.8\times10^3$ km^2, and the Pacific Ocean (receiving five rivers) has the lowest annual-mean plume area of 421×10^3 km^2. Although the Indian Ocean has lower annual discharge than the Pacific, its annual-mean plume area is much larger than that of the Pacific. Moreover, the annual-mean plume area in the tropical zone (including eight rivers)

Table 3. The monthly plume areas of world's 19 major rivers (unit: 10^3 km^2)

River	January	February	March	April	May	June	July	August	September	October	November	December	Annual mean	Rank of discharge
Amazon 1 (S <32)	179.7	211.3	234.3	322.4	401.4	276.1	261.7	229.5	149.0	99.9	112.4	146.2	218.7	1
Congo 2 (S <32)	80.0	98.3	139.4	64.6	34.3	18.4	14.0	15.1	15.7	24.8	40.9	66.4	51.0	2
Orinoco 3 (S <32)	6.4	Null	Null	12.2	6.4	Null	32.8	71.6	80.7	57.3	43.2	38.3	38.8	3
Mississippi 7 (S <32)	34.1	43.3	55.4	59.7	134.2	155.6	138.7	109.8	37.3	21.1	23.6	30.8	70.3	7
Paraná 10 (S <32)	127.0	118.2	120.8	135.4	82.8	60.0	89.3	143.1	150.1	129.3	115.3	121.6	116.1	10
Saint Lawrence 11 (S <32)	411.0	350.8	346.4	378.5	404.9	571.1	462.9	828.3	748.1	667.9	569.4	471.6	517.6	11
Niger 24 (S <32)	235.2	153.6	171.0	191.7	123.4	46.0	70.7	61.5	25.4	107.7	227.0	256.0	139.1	24
Changjiang 5 (S <31)	128.4	120.3	123.4	133.4	152.3	188.3	391.7	421.1	368.9	276.6	165.5	230.2	225.0	5
Amur 14 (S <31)	87.3	84.8	Null	Null	80.3	119.8	154.1	110.3	100.3	91.4	65.8	75.2	96.9	14
Zhujiang 16 (S <31)	1.9	1.7	1.9	8.6	10.1	42.5	65.7	19.1	29.1	23.7	Null	Null	20.4	16
Columbia 18 (S <31)	14.1	15.6	14.1	26.0	38.2	39.1	32.3	5.3	4.3	4.9	2.4	7.7	17.0	18
Yukon 23 (S <31)	38.9	34.5	15.8	7.8	23.3	142.0	117.0	176.2	112.4	127.5	102.1	67.4	81.2	23
Ganges and Brahmaputra, Irrawaddy and Salween 4, 12, 17 (S <32)[1)]	743.1	274.1	159.7	152.7	178.6	280.0	394.1	952.7	1 082.5	1 016.6	1 267.2	1 377.8	656.6	4, 12, 17
Yenisei and Ob 6, 8 (S <27)	267.5	358.0	280.5	155.0	23.0	170.4	294.7	398.0	331.4	196.8	166.5	169.6	234.3	6, 13
Lena and Kolyma 13 (S <27)	1 006.5	1 014.4	962.1	613.4	22.9	1 610.5	1 661.5	1 399.9	1 059.5	1 239.9	1 266.1	1 096.1	1 079.4	8
Mackenzie 15 (S <27)	72.3	61.4	64.1	1.5	Null	322.9	573.9	435.7	261.1	103.2	162.5	125.9	198.6	15
Total	3 433.4	2 940.3	2 688.9	2 262.9	1 716.1	4 042.7	4 755.1	5 377.2	4 564.8	4 188.6	4 329.9	4 280.8	3 715.1	

Notes: S means the salinity threshold for the plume detection. [1)] These rivers are much too close to each other, and it is hard to separate the plume area of the individual river, so we calculated the total plume area as a whole.

Table 4. The plume areas of world's 19 major rivers according to the receiving oceans and latitude zones (unit: 10^3 km^2)

Ocean name	January	February	March	April	May	June	July	August	September	October	November	December	Annual mean	Discharge/ 10^9 m^3·a^{-1}	Salinity threshold
Atlantic	1 073.4	975.5	1 067.3	1 164.5	1 187.4	1 127.2	1 070.1	1 458.9	1 206.3	1 108	1 131.8	1 130.9	1 141.8	10 390	32
Pacific	270.6	256.9	155.2	175.8	304.2	531.7	760.8	732.0	642.0	524.1	335.8	380.5	421	1 970	31
Indian Ocean	743.1	274.1	159.7	152.7	178.6	280	394.1	952.7	1 082.5	1 016.6	1 267.2	1 377.8	656.6	1 700	32
Arctic latitude zonal	1 346.3	1 433.8	1 306.7	769.9	45.9	2 103.8	2 530.1	2 233.6	1 652	1 539.9	1 595.1	1 391.6	1 495.7	1 850	27
60°–90° (polar)	1 346.3	1 433.8	1 306.7	769.9	45.9	2 103.8	2 530.1	2 233.6	1 652	1 539.9	1 595.1	1 391.6	1 495.7	1 850	31, 32
30°–60° (temperate)	840.8	767.5	675.9	740.8	916.0	1 275.9	1 386.0	1 794.1	1 530.4	1 318.7	1 044.1	1 004.5	1 107.9	3 120	31, 32
30°–30° (tropical)	1 246.3	739	706.3	752.2	754.2	663.0	839	1 349.5	1 382.4	1 330	1 690.7	1 884.7	1 111.4	10 940	27

is much larger than that in the temperate zone (including seven rivers). As for the polar region, the annual discharge is $1\,850\times10^9$ km^3, which is only about 11.6% of the total discharge of the 19 rivers. However, the annual-mean plume area in the Arctic Ocean is up to $1\,495.7\times10^3$ km^2, indicating the large contribution of ice melt. Therefore, one must be cautioned if one wants to the use this plume area to calculate the fluxes of terrestrial material into the Arctic Ocean.

3.2 *Seasonal variation of global major river plume areas*

Figure 2 shows the seasonal distributions of the plume regions corresponding to the 19 rivers, with February, May, August and November representing the winter, spring, summer, and autumn in the Northern Hemisphere, respectively. Clearly, there are significant seasonal variations in the river plume areas, especially in the moderate to high latitude regions. More specifically, Fig.3 gives the details of the monthly plume areas variations for the Amazon, Orinoco, Changjiang, and Mississippi Rivers. For the Amazon River, the maximum plume area occurs in May and the minimum in October. In contrast, for the Orinoco River located north of the Amazon River, the maximum plume area occurs in September. The Changjiang and Mississippi Rivers are the two large rivers in the temperate latitudes of the Northern Hemisphere, and their largest plume areas occur in the summer due to the large river discharges associated with their wet seasons (see the next section for details). Therefore, different rivers have different seasonal variations in terms of the river plume area, and the magnitudes of the plume area in each month for all 19 rivers are given in Table 3. The maximum value for the total area of these river plumes is 5.38×10^6 km^2 in August, and the minimum value is 1.72×10^6 km^2 in May.

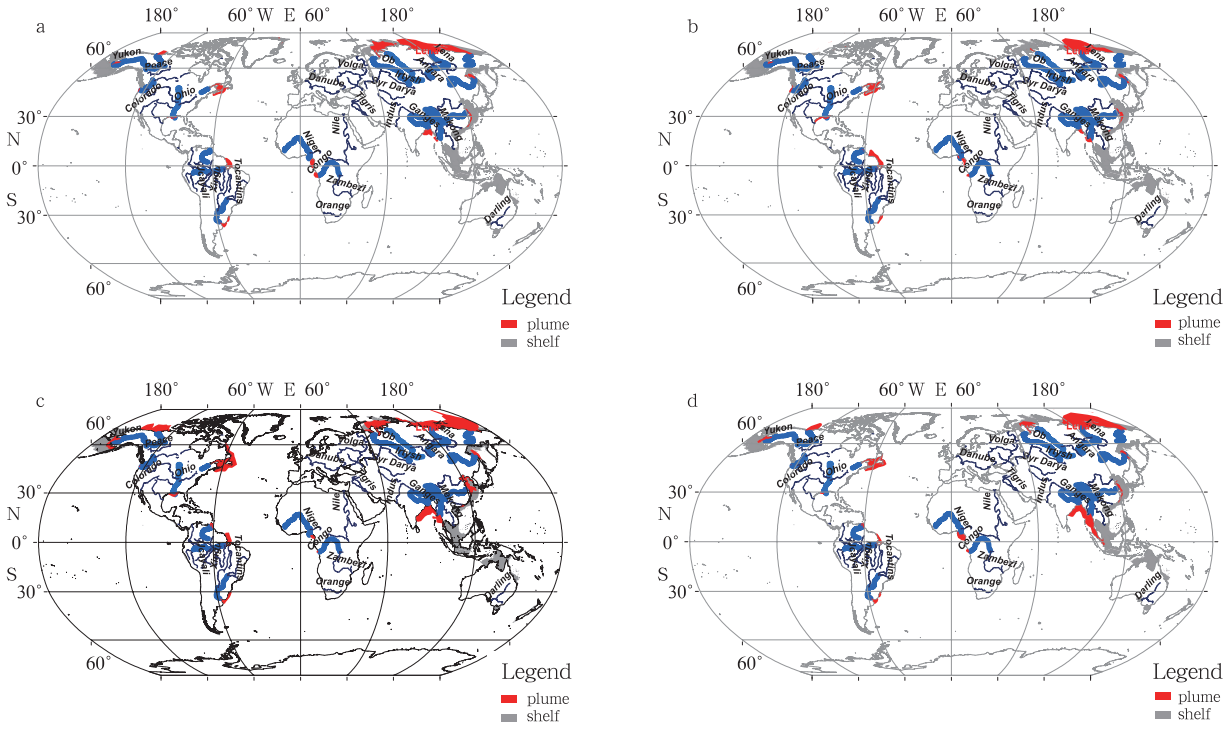

Fig.2. Seasonal distributions of the plume regions corresponding to the world's 19 major rivers, with February (a), May (b), August (c) and November (d) representing the winter, spring, summer, and autumn in the Northern Hemisphere, respectively.

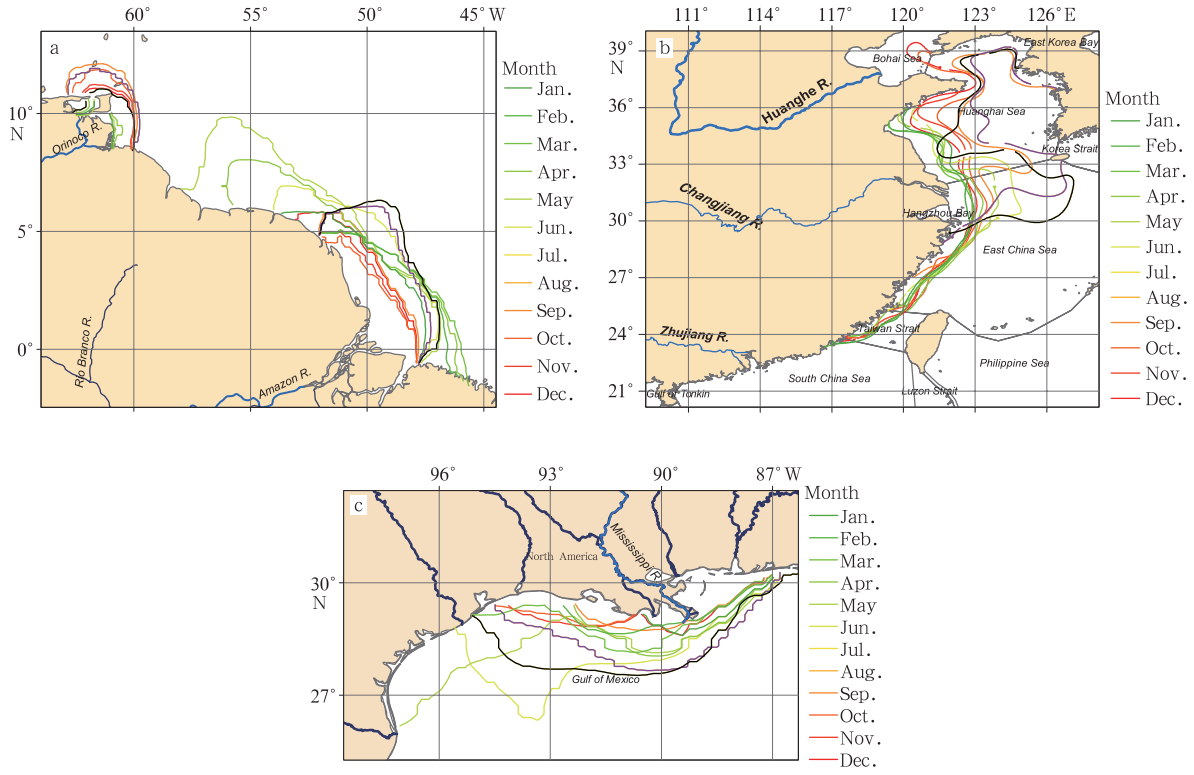

Fig.3. Monthly variations of the plume areas for the Amazon and Orinoco rivers (a), the Changjiang River (b) and the Mississippi River (c). The color bar shows the months from January to December.

3.3 *Relationship between plume area and river discharge*

Except for the huge ice melt in the polar region, the freshwater in plume regions is mainly from river input. Therefore, plume area is expected to be primarily controlled by river discharge. Figure 4 shows linear regressions between monthly plume areas and river discharges for the individual river, excluding those entering the Arctic Ocean. Generally, the plume area increases with increasing river discharge for all 16 rivers, except for the Parana River located in the SE of South America (Fig.1). The linear relationship between the monthly plume areas and river discharge is quite good for the Amazon River. For the remaining 15 rivers, however the linear relationship is not good, indicating the impacts of the other factors on the size of the plume, such as coastal currents, wind speed and direction, tidal movement and the change of the shoreline etc. (Dagg et al., 2004). Schettini et al. (1998) and Dagg et al. (2004) classified plumes into two types: riverine plumes (e.g., Mississippi and Amazon Rivers) and estuarine plumes (e.g., St. Lawrence River). For the riverine plume, the freshwater from the river is directly injected over the shelf, and the salinity and other riverine materials usually have strong gradients. For the estuarine plumes, the freshwater released into the adjacent sea already has a significant contribution of salt water before being released to the shelf. Therefore, the estuarine plume often has larger areas than the riverine plume if other conditions are the same.

It is interesting to note that, although for each river the correlation between the monthly plume area and discharge is reasonably good, large rivers, such as the Amazon, Congo, and Orinoco, do not necessarily have large plume areas compared with many small rivers. The reasons behind this need further investigation.

3.4 *Impact of the threshold salinity on the plume area extraction*

Figure 5 shows examples of the variation of plume area's variation when different threshold salinities are implied in August. Clearly, the plume areas of high latitude rivers, especially those in the Arctic Ocean, increase rapidly with threshold salinity. The increasing slopes of the river plume area that occur with an increase of the threshold salinity for the Amazon, Orinoco, Parana, and Niger Rivers are relatively flat compared with higher latitude rivers, indicating the sharp salinity gradients at the boundaries of these river plumes. In addition, due to the relatively large slopes, the selection of the threshold salinity is important for defining of the river plumes of high latitude rivers.

3.5 *Comparison of GIS-extracted areas with literature's results*

First, based on the basic geographic information data and ArcGIS analysis, we calculated the total surface area of the global ocean to be 365.051×10^6 km^2. This result is quite similar to Feng's (Feng et al., 2004) result of 361.059×10^6 km^2, with a relative difference of 1.1%. We also calculated the total area of global continental shelves with water depths less than 200 m, and the result is 26.15×10^6 km^2, which is also quite similar to the value of 24.7×10^6 km^2 used by Laruelle et al. (2010). Actually, the area used by Laruelle et al. (2010) was approximated by multiplying cell counts with per-cell areas. The good agreement both for the areas of the global ocean area and the global continental shelves gives credit to the area extracted by the GIS technique.

Due to the highly dynamic feature of river plumes both in

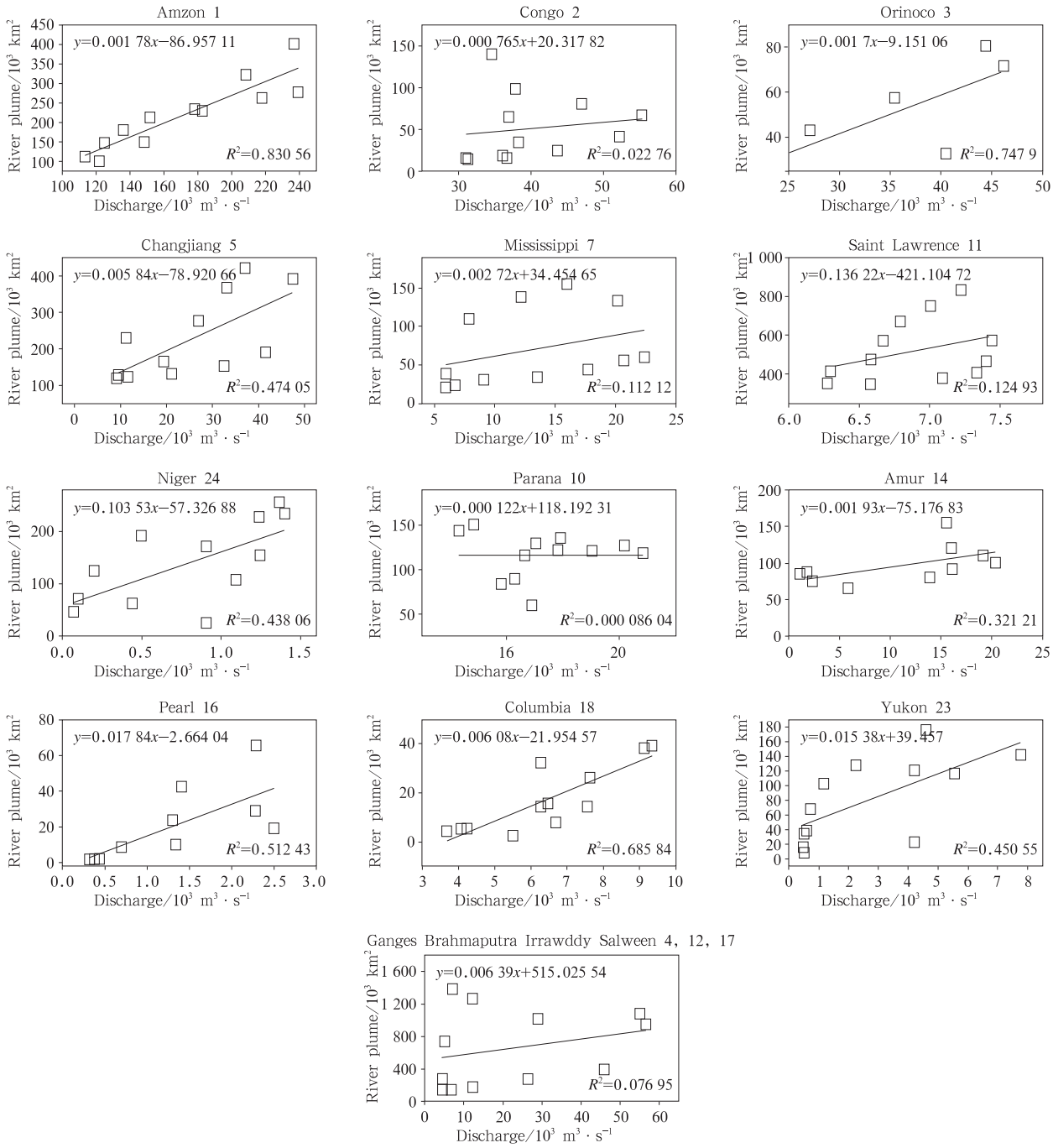

Fig.4. Linear regressions between monthly plume areas and river discharges for the world's 16 largest rivers. Rivers discharging into the Arctic Ocean are excluded. The number next to the river name denotes its rank in terms of discharge.

space and time, it is difficult to identify the plume area using field surveys. Up to now, only very few data concerning the global major river plume areas can be found. Molleri et al. (2010) used the relationship between sea-surface salinity (SSS) and the absorption coefficient of dissolved and detrital material from the satellite ocean color sensor SeaWiFS (Sea-viewing Wide Field-of-view Sensor) to identify the Amazon River plume, and they obtained a maximum plume area of 1 506×10³ km² from July to August for regions with a salinity less than 34. Based on the WOA09 salinity data set and the GIS method, we obtained a very similar mean plume area (with salinity less than 34) of 1 457.4×10³ km² for Amazon River from June to August, with 1 941.9×10³ km² in June, 1 409.2×10³ km² in July, and 1 020.9×10³ km² in August. On the other hand, Gupta and Krishnan (1994) gave the areas of selected sediment plumes of South and Southeast Asia, and among them, the Ganga-Brahmaputra and Irrawaddy-Salween River plume areas were reported as 40.444 3×10³ km² and 40.645×10³ km² (Gupta and Krishnan, 1994), respectively. These values are much smaller than our results (the minimum is 152.7×10³ km² in April and

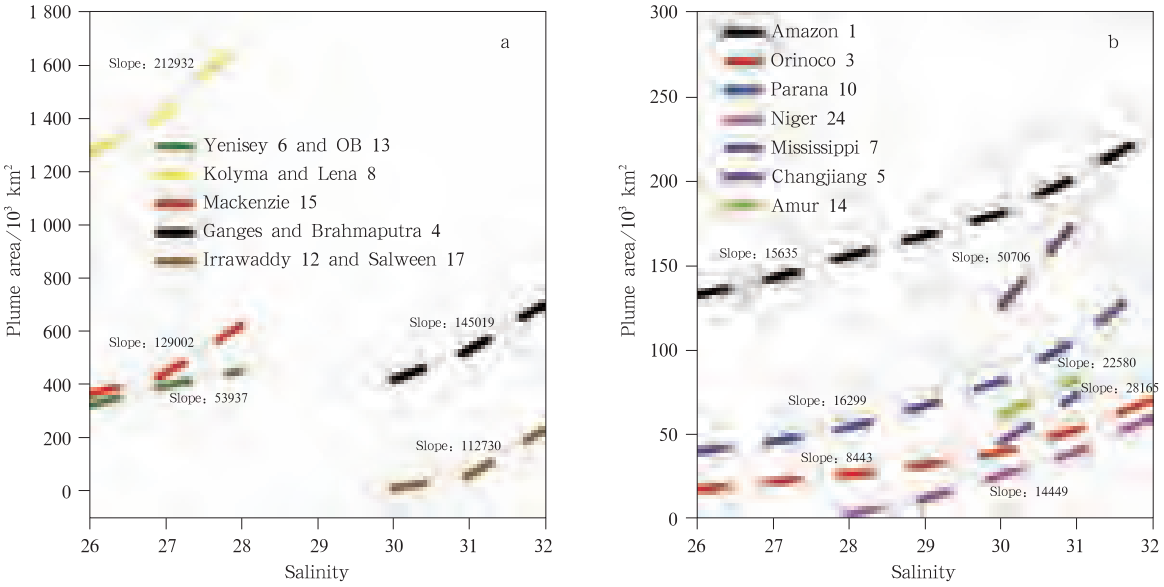

Fig.5. The variation of plume area with different threshold salinities in August. Linear regression equations correspond to: Plume area = offset + slope × salinity. a. Five rivers flowing into the Arctic and Indian Oceans have small slops, and b. eight rivers flowing into the Atlantic and Pacific Oceans have large slopes. The number next to the river name denotes its rank in terms of discharge.

the maximum is 1 377.8×10³ km² in December) (Table 3). The likely explanation is that the low salinity water spreads much more widely than the sediments, hence the plume area is larger when based on salinity.

4 Summary and implications

Based on the climatological salinity data set (from NOAA WOA09 and Chinese ocean atlas) and a GIS technique, the plume areas of the world's 19 major rivers were extracted in this study. The maximum value for the total areas of these river plumes is 5.38×10⁶ km² in July, and the minimum value is 1.72×10⁶ km² in May. The annual mean area of these river plumes is 3.72×10⁶ km², and they take up approximately 14.2% of the total continental shelf area. We also present statistics describing river plume areas for different oceans and latitude zones, and we analyze the seasonal variations of the plume areas and their relationships with river discharge.

The amount of riverine materials, including the sediment, carbon and nutrients, transported with the plume can travel long distances and significantly influence the continental shelf and the surrounding ocean. Thus, the spatial patterns of plume extension and the total areas are relevant to many specific prossesses that greatly impact human society, such as the possibility of hypoxia, air-sea CO_2 flux, fishery productivity and so forth. However, the plume area is too difficult to estimate from limited field investigations. Our data for the 19 largest river plume areas are necessarily only a crude estimate. Nevertheless, this study has provided a useful basic data set for the first time, and it should have wide implications for studies in the marginal seas.

In large river plume systems, consumption of oxygen in bottom waters is linked to biological oxygen demand fueled by organic matter from primary production in the nutrient-rich river plume and perhaps also to terrigenous inputs (Rabouille et al., 2008). When the water column structure is stratified, it often results in low dissolved oxygen concentrations (hypoxia) in estuaries and semi-enclosed seas throughout the world (Breitburg et al., 2010). Thus, the plume area and location would indicate position of low oxygen bottom areas to some extent.

A more direct use of the plume area is the global estimation of the CO_2 budget. The total CO_2 sink (calculated by carbon) in open ocean is estimated to rang from –1.4 Pg/a to –2.2 Pg/a (Gruber et al., 2009; Takahashi et al., 2009). However, in continental shelves which cover only about 7% of the global ocean area, estimates of the CO_2 sink are converging around –0.22– –0.45 Pg/a in recent publications (Thomas et al., 2004; Borges et al., 2005; Cai et al., 2006; Chen and Borges, 2009; Laruelle et al., 2010). These data still have large uncertainties, and the different areas used to describe the highly dynamic plumes are major sources of the uncertainty. Recently, studies of carbon fluxes for some river plumes were carried out on the basis of very limited in situ data. In the Amazon River plume for instance, the mean uptake rates of atmospheric CO_2 (calculated by carbon) are about –0.5 mol/(m²·a) in summer (Ternon et al., 2000; Kortzinger, 2003), and –4– –7 mmol/(m²·d) in autumn (Cooley et al., 2007). The mean uptake rates of atmospheric CO_2 in the Changjiang River plume are –3.4– –8.0 mmol/(m²·d) (Tsunogai et al., 1999; Wang et al., 2000). For the Mississippi River plume, the mean uptake rates of the atmospheric CO_2 are –1.39– –2.96 mmol/(m²·d) in August 2004 and April 2006 (Lohrenz and Cai, 2010). However, due to the lack of available plume areas for global rivers and also sufficient in situ data sets, synthetic estimation of the CO_2 budget for global river plumes is still not possible. Thus, our plume areas statistics could provide an important basic data set for the estimation of the CO_2 budget of global river plumes.

Acknowledgements

The authors would like to thank NOAA for providing the World Ocean Atlas 2009 (WOA09) data set and the State Oceanic Administration of China for providing the Marine Atlas of China sea data. The Nature Earth and the Rivers Discharge Database is also thanked for providing base geospatial data and month

discharge data respectively.

References

Antonov J I, Seidov D, Boyer T P, et al. 2010. World Ocean Atlas 2009, 2(Salinity). NOAA Atlas NESDIS 69. Washington D C: Government Printing Office, 184

Binding C E, Bowers D G. 2003. Measuring the salinity of the Clyde Sea from remotely sensed ocean colour. Estuarine, Coastal and Shelf Science, 57(4): 605–611

Borges A V, Delille B, Frankignoulle M. 2005. Budgeting sinks and sources of CO_2 in the coastal ocean: Diversity of ecosystems counts. Geophysical Research Letters, 32: L14601

Breitburg D L, Crump B C, Dabiri J O, et al. 2010. Ecosystem engineers in the plankton: Habitat alteration by species ranging from microbes to jellyfish. Integrative and Comparative Biology, 50(2): 188–200

Cai Weijun. 2003. Riverine inorganic carbon flux and rate of biological uptake in the Mississippi River plume. Geophysical Research Letters, 30(2): 1032

Cai Weijun, Dai Minghan, Wang Yongchen. 2006. Air-sea exchange of carbon dioxide in ocean margins: a province-based sysnthesis. Geophysical Research Letters, 33: L12603

Chen Daxi. 1992. Marine atlas of the Bohai Sea, Yellow Sea and East China Sea—Hydrology. In: Chen Guozheng, ed. Marine Atlas of the Bohai Sea, Yellow Sea and East China Sea (in Chinese). Beijing: China Ocean Press, 97–163

Chen Chen-Tung Arthur, Borges A V. 2009. Reconciling opposing views on carbon cycling in the coastal ocean: continental shelves as sinks and near-shore ecosystems as sources of atmospheric CO_2. Deep Sea Research Part II, 56(8–10): 578–590

Chen Zhiqiang, Hu Chuanmin, Conmy R N, et al. 2007. Colored dissolved organic matter in Tampa Bay, Florida. Marine Chemistry, 104(1–2): 98–109

Chen Chen-Tung Arthur, Huang TingHsuan, Fu YuHan, et al. 2012. Strong sources of CO_2 in upper estuaries become sinks of CO_2 in large river plumes. Environmental Sustainability, 4(2): 179–185

Chen Chen-Tung Arthur, Zhai Weidong, Dai Minghan. 2008. Riverine input and air-sea CO_2 exchanges near the Changjiang (Yangtze River) Estuary: Status quo and implication on possible future changes in metabolic status. Continental Shelf Research, 28: 1476–1482

Cooley S R, Coles V J, Subramaniam A, et al. 2007. Seasonal variations in the Amazon plume-related atmospheric carbon sink. Global Biogeochemical Cycles, 21: GB3014

Dagg M, Benner R, Lohrenz S, et al. 2004. Transformation of dissolved and particulate materials on continental shelves influenced by large rivers: Plume processes. Continental Shelf Research, 24: 833–858

Diaz R J, Rosenberg R. 2008. Spreading dead zones and consequences for marine ecosystems. Science, 321(5891): 926–929

D'Sa E J, Miller R L. 2003. Bio-optical properties in waters influenced by the Mississippi River during low flow conditions. Remote Sensing of Environment, 84(4): 538–549

Dzwonkowski B, Yan X H. 2005. Tracking of a Chesapeake Bay estuarine outflow plume with satellite-based ocean color data. Continental Shelf Research, 25(16): 1942–1958

Feng Shizuo, Li Fengqi, Li Shaoqing. 2004. An Introduction to Marine Science (in Chinese). Beijing: Higher Education Press, 22

Font J A, Camps A. 2010. SMOS: The challenging sea surface salinity measurements from space. In: Borges A, Martín-Neira M, Boutin J, et al., eds. IEEE, 98(5): 649–665

GRDC. 2009. Global Runoff Data Centre (2009): Surface Freshwater Fluxes into the World Oceans/GRDC. Koblenz, Germany: Federal Institute of Hydrology (BfG)

Green R E, Bianchi T S, Dagg M J, et al. 2006. An organic carbon budget for the Mississippi River turbidity plume and plume contributions to air-sea CO_2 fluxes and bottom water hypoxia. Estuaries and Coasts, 29(4): 579–597

Gruber N, Gloor M, Mikaloff F S E, et al. 2009. Oceanic sources, sinks, and transport of atmospheric CO_2. Global Biogeochem Cycles, 23(2009): GB1005

Gupta A, Krishnan P. 1994. Spatial distribution of sediment discharge to the coastal waters of South and Southeast Asia. International Association of Hydrological Sciences, Publication 224. Oxfordshire, UK: Wallingford

Higgins H W, Mackey D J, Clementson L. 2006. Phytoplankton distribution in the Bismarch Sea North of Papua New Guinea: The effect of the Sepik River outflow. Deep–Sea Research Part I, 53(11): 1845–1863

Hou Wenfeng. 2006. Marine Atlas of the North China Sea—Hydrology. In: Li Tingdong, ed. Marine Atlas of the North China Sea. Beijing: China Ocean Press, 148–165

Hu C, Montgomery E T, Schmitt R W, et al. 2004. The dispersal of the Amazon and Orinoco River water in the tropical Atlantic and Caribbean Sea: observation from space and S-PALACE floats. Deep–Sea Research Part II, 51(10–11): 1151–1171

Jo Y H, Yan X H, Dzwonkowski B, et al. 2005. A study of the freshwater discharge from the Amazon River into the tropical Atlantic using multi-sensor data. Geophysical Research Letters, 32: L02605

Kerr Y, Waldteufel P, Wigneron J P, et al. 2010. The SMOS Mission: New Tool for Monitoring Key Elements of the Global Water Cycle. Proceedings of the IEEE, 98(5): 666–687

Kim H C, Yamaguch H, Yoo S, et al. 2009. Distribution of Changjiang diluted water detected by satellite chlorophyll- and its interannual variation during 1998–2007. Journal of Oceanography, 65(2009): 129–135

Klemas V. 2012. Remote sensing of coastal plumes and ocean fronts: overview and case study. Journal of Coastal Research, 28(1A): 1–7

Koblinsky C J, Hildebrand P, LeVine D, et al. 2003. Sea surface salinity from space: Science goals and measurement approach. Radio Science, 38(4): 8064

Kortzinger A. 2003. A significant CO_2 sink in the tropical Atlantic Ocean associated with the Amazon River plume. Geophysical Research Letters, 30(24): 2287

Kouame K V, Yapo O B, Mambo V, et al. 2009. Physicochemical characterization of the waters of the coastal rivers and the lagoonal system of cote d'Ivoire. Journal of Applied Sciences, 9(8): 1517–1523

Laruelle G G, Dürr H H, Slomp C P, et al. 2010. Evaluation of sinks and sources of CO_2 in the global coastal ocean using a spatially-explicit typology of estuaries and continental shelves. Geophysical Research Letters, 37: L15607

Lihan T, Saitoh S I, Iida T, et al. 2008. Satellite-measured temporal and spatial variability of the Tokachi River plume. Estuarine, Coastal and Shelf Science, 78(2): 237–249

Lique C, Garric G, Treguier A M, et al. 2011. Evolution of the arctic ocean salinity, 2007–08: contrast between the canadian and the eurasian basins. Journal of Climate, 24(6): 1705–1717

Lohrenz S E, Cai W J, et al. 2010. Seasonal variability in air-sea fluxes of CO_2 in a river-influenced coastal margin. Journal of Geophysical Research-Oceans, 115(C10): C10034

McKee B A. 2003. RiOMar: The Transport, Transformation and Fate of Carbon in River-dominated Ocean Margins. Report of the RiOMar Workshop. New Orleans, LA: Tulane University

Molleri G S F, Novo E M L, Kampel M. 2010. Space-time variability of the Amazon River plume based on satellite ocean color. Continental Shelf Research, 30(3–4): 342–352

Piola A R, Romero S I, Zajaczkovski U. 2008. Space-time variability of the Plata plume inferred from ocean color. Continental Shelf Research, 28(13): 1556–1567

Rabouille C, Conley D J, Dai M H, et al. 2008. Comparison of hypoxia among four river-dominated ocean margins: the Changjiang (Yangtze), Mississippi, Pearl, and Rhone rivers. Continental Shelf Research, 28: 1527–1537

Schettini C A F, Kuroshima K N, Pereira Filho J, et al. 1998. Oceanographic and ecological aspects of the Itajaí-açu river plume during a high discharge period. Anais Acad Bras Ciênc, 70(2): 335–351

Shipe R F, Curtaz J, Subramaniam A, et al. 2006. Diatom biomass and productivity in oceanic and plume-influenced waters of the western tropical Atlantic ocean. Deep–Sea Research Part I, 53: 1320–1334

Smith Jr W O, Demaster D J. 1996. Phytoplankton biomass and productivity in the Amazon River plume: Correlation with seasonal river discharge. Continental Shelf Research, 16: 291–319

Takahashi T, Sutherland S C, Wanninkhof R, et al. 2009. Climatological mean and decadal changes in surface ocean pCO_2, and net sea-air CO_2 flux over the global oceans. Deep–Sea Research Part II, 56(8–10): 554–577

Tan Yan, Zhang Longjun, Wang Fan, et al. 2004. Summer surface water pCO_2 flux at air-sea interface in western part of the East China Sea. Oceanologia et Limnologia Sinica (in Chinese), 35(3): 239–245

Ternon J F, Oudot C, Dessier A, et al. 2000. A seasonal tropical sink for atmospheric CO_2 in the Atlantic Ocean: the role of the Amazon River discharge. Marine Chemistry, 68: 183–201

Thomas H, Bozec Y, Elkalay K et al. 2004. Enhanced open ocean storage of CO_2 from shelf sea pumping. Science, 304: 1005–1008

Thomas A C, Weatherbee R A. 2006. Satellite-measured temporal variability of the Columbia River plume. Remote Sensing of Environment, 100(2): 167–178

Tsunogai S, Watanabe S, Sato T. 1999. Is there a "continental shelf pump" for the absorption of atmospheric CO_2? Tellus, 51(B): 701–712

Vecchio R D, Subramaniam A. 2004. Influence of the Amazon River on the surface optical properties of the western tropical North Atlantic Ocean. Journal of Geophysical Research, 109(C11001): 1–13

Walker N D. 1996. Satellite assessment of Mississippi River plume variability: causes and predictability. Remote Sensing of Environment, 58(1): 21–35

Wang S L, Chen C T A, Hong G H, et al. 2000. Carbon dioxide and related parameters in the East China Sea. Continental Shelf Research, 20: 525–544

Zhai Weidong, Dai Minghan. 2009. On the seasonal variation of air-sea CO_2 fluxes in the outer Changjiang (Yangtze River) Estuary, East China Sea. Marine Chemistry, 117(1–4): 2–10

Zhai Weidong, Dai Minghan, Cai Weijun. 2009. Coupling of surface pCO_2 and dissolved oxygen in the northern South China Sea: impacts of contrasting coastal processes. Biogeosciences, 6: 2589–2598